NEUROPHYSIOLOGY

Subdomains within orientation columns of primary visual cortex

Ming Li[1]*, Xue Mei Song[2,3]*, Tao Xu[2,4,5], Dewen Hu[1]†, Anna Wang Roe[3]†, Chao-Yi Li[1,2,4]‡

In the mammalian visual system, early stages of visual form processing begin with orientation-selective neurons in primary visual cortex (V1). In many species (including humans, monkeys, tree shrews, cats, and ferrets), these neurons are organized in a beautifully arrayed pinwheel-like orientation columns, which shift in orientation preference across V1. However, to date, the relationship of orientation architecture to the encoding of multiple elemental aspects of visual contours is still unknown. Here, using a novel, highly accurate method of targeting electrode position, we report for the first time the presence of three subdomains within single orientation domains. We suggest that these zones subserve computation of distinct aspects of visual contours and propose a novel tripartite pinwheel-centered view of an orientation hypercolumn.

INTRODUCTION

Orientation selectivity of neurons in V1 is believed to be central to visual form perception. Their regular organization portrayed in orientation maps has been known for several decades and have become a cornerstone of cortical organization (1–3). Within orientation maps, neuronal orientation preference shifts across cortical space, highlighted by locations of orientation singularities termed orientation pinwheels. However, despite the rich literature on visual contour processing, there is little understanding on how functional architecture within single orientation columns may contribute to the generation of different elemental aspects of visual contours (such as linear oriented segments, curved segments, corners, and T junctions) (4–7).

Previous studies have shown that two regions of orientation maps, orientation domains and pinwheel regions, are distinct, and some of these findings support two-stage models of contour integration [e.g., (8)]. Here, based on multiple functional parameter assessment (receptive field size, orientation tuning width, surround suppression characteristics, latency to response, and spatiotemporal frequency preference), we report for the first time the presence of three functional zones within single orientation columns. The key to this study is the development of a highly accurate method of targeting electrode position, thereby enabling distinctions within single orientation column locations. We suggest that the functional properties within these three zones support a three-stage model of visual contour processing in V1.

RESULTS

Defining subregions within the orientation map: pinwheel center, domain midway, and domain point

After obtaining orientation maps in cat V1 with intrinsic signal optical imaging (Fig. 1, A and B), we selected two neighboring pinwheel

centers (PCs; points 1 and 2 in Fig. 1C) and defined three evenly spaced points along the intervening iso-orientation domain: domain point (DP; the center point between the two neighboring PCs; point 3 in Fig. 1C) and domain midway (DM; midway between PC and DP; points 4 and 5 in Fig. 1C). We chose only highly accurate and reproducible maps, i.e., those in which there was no displacement of PCs between two repeated maps (9). We also took extra efforts to ensure that the electrode penetration was perpendicular to the cortical surface (fig. S1) by imaging a large field of view with a narrow depth of field (~50 μm), providing a <2° deviation from perpendicular. At each of these locations, we recorded single-unit responses and local field potentials (LFPs). For each neuron recorded, we determined multiple properties: preferred orientation, optimal spatial frequency (SF) and temporal frequency (TF), location and size of the classical receptive field (CRF), surround suppression characteristics, response latency, and so on. In the following sections, we describe the differences observed between neurons in the PC, DM, and DP locations.

Highly accurate quantitative determination of PC locations

To study the functional organization within single orientation domains, it was important to target pinwheel substructures with accuracy. Previous studies relied solely on blood vessel images of the cortical surface to guide electrode penetrations to locations in the orientation maps (Fig. 1, A and B). However, considerable spatial error remains using this method (10). In the present study, we improved the accuracy of targeting PC locations by using the orientation tuning of LFP recorded at or near the optically determined positions. The procedure is described below.

As shown previously, the orientation tuning of LFPs recorded in orientation domains are well fit by sine waves, while those in PCs, because of the presence of different orientation preferences, are not sine-like (11). We reasoned that the center of the pinwheel can be accurately determined by finding the location with non–sine-like LFP orientation tuning.

To quantitatively estimate the unlikeness of the LFP curve to sine waves, we presented the non–sine-like index (NSI), which is defined as the P value of a surrogate data test (see Data analysis section in Materials and Methods). NSI ranged from 0 to 1, with 0 as highly sine-like and 1 as highly non–sine-like. To determine the NSI threshold for discriminating sine from non-sine curves and non-PC from PC sites, we studied the relationship between NSI and the maximal orientation scatter (MOS; the biggest preferred orientation difference among all the

[1]College of Intelligence Science and Technology, National University of Defense Technology, Changsha 410073, China. [2]Shanghai Institutes of Biological Sciences, Chinese Academy of Sciences, Shanghai 200031, China. [3]Interdisciplinary Institute of Neuroscience and Technology, Second Affiliated Hospital, School of Medicine, Zhejiang University, Hangzhou 310029, China. [4]Key Laboratory for Neuroinformation of Ministry of Education, University of Electronic Science and Technology of China, Chengdu 610054, China. [5]School of Ophthalmology and Optometry, Wenzhou Medical University, Wenzhou 325027, China.
*These authors contributed equally to this work.
†Corresponding author. Email: annawang@zju.edu.cn (A.W.R.); dwhu@nudt.edu.cn (D.H.)
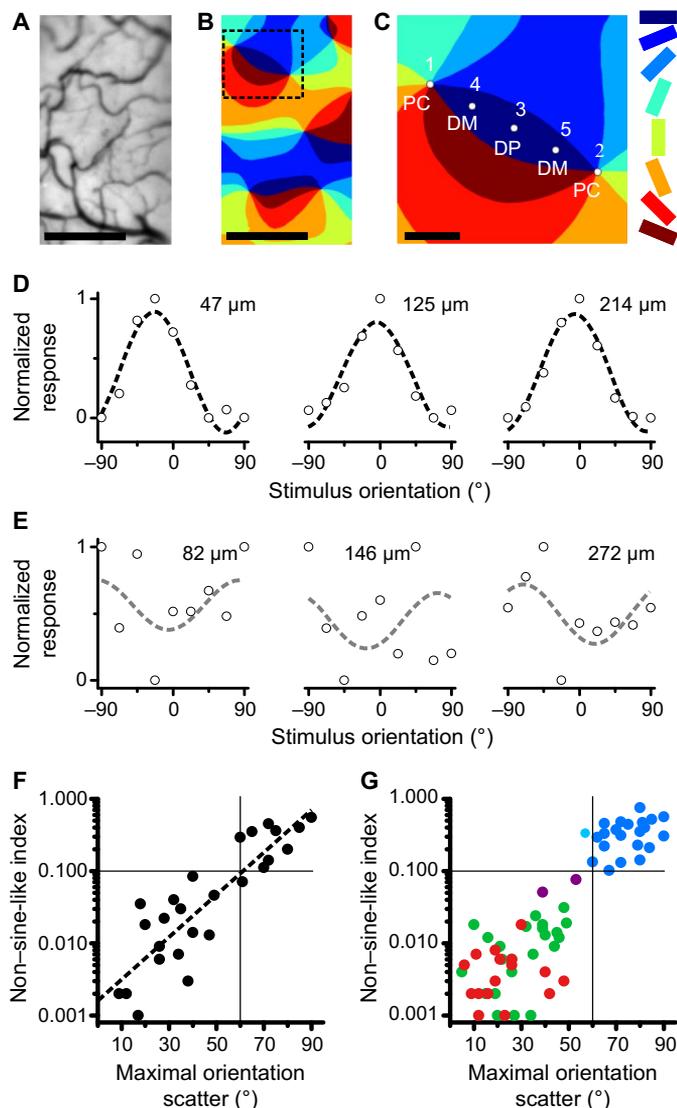‡Deceased.

Fig. 1. Highly accurate and quantitative determination of PC locations. (**A**) Vascular pattern of the cortical surface. (**B**) The color-coded orientation map of the cortex in (A). (**C**) Two neighboring PCs (locations 1 and 2) and three evenly spaced intervening points (DP, location 3; DM, locations 4 and 5) in the orientation domain. The eight stimulus orientations are color coded at 22.5° intervals. Scale bars, 500 μm (A and B) and 100 μm (C). (**D**) Examples of the sine-like LFP orientation-tuning curve at false PC sites. The three LFP curves were recorded at a false PC site [maximal orientation scatter (MOS) = 18°] in depths of 47, 125, and 214 μm from the pial surface, respectively. Their non–sine-like index (NSI) values are all 0 (highly sine-like). (**E**) Examples of the non–sine-like LFP orientation-tuning curve at true PC sites. The three LFP curves were obtained at depths of 82, 146, and 272 μm, respectively, at a true PC site (MOS = 65°). Their NSI values are 0.34, 0.46, and 0.32, respectively. (**F**) Determining the NSI threshold for PCs. (**G**) Application of the NSI threshold to recorded sites and the population of cells recorded at sites of PC, DM, and DP, which are targeted using LFP methods.

neurons recorded in one site) in five cats. MOS is one of the most reliable indices for identifying PCs and is larger than 60° only at the very center of PC sites (*12*).

Targeting PCs purely using blood vessel maps, we recorded three or more cells within each penetration to the putative PCs and then

calculated the MOS value by finding the biggest preferred orientation difference between any two of these cells. In addition, we recorded the orientation tuning of the LFP. A total of 26 putative PC sites in five cats were targeted, and 86 neurons and 86 LFP curves were recorded. It is consistently found that, when the electrodes were guided to the false PC sites (MOS < 60°), the LFP curves are sine-like (see the examples in Fig. 1D), and at the true PC sites (MOS ≥ 60°), the LFP curves are non–sine-like (see the examples in Fig. 1E).

Using the NSI to measure the non–sine-likeness of each LFP curve, we plotted the NSI versus MOS for all the 26 sites in Fig. 1F. It can be seen that there is a positive relationship between NSI and MOS. We consistently observed that, when the NSI was greater than 0.1, the MOS was greater than ~60°, confirming that an NSI threshold of 0.10 corresponds to the PC.

After determining the threshold, we then started our study on functional organization within orientation domains and targeted pinwheel locations using our LFP method. A total of 195 neurons were recorded at 70 sites (including PC, DM, and DP) in 11 cats. We observed that almost all cells recorded in PC locations (indicated by NSI > 0.1) have MOS larger than 60° (blue dots) [except one, MOS = 57° (light blue dot)], and almost all cells recorded in DM (green dots) and DP (red dots) locations are with NSI < 0.05 [except one DM, NSI = 0.076 and one DP, NSI = 0.051 (purple dots)] (Fig. 1G). We included in our analysis only cells with NSI > 0.1 (PC cells) or NSI < 0.05 (DM or DP cells), excluding cells in the intermediate zone. Thus, we are highly confident about our PC, DM, and DP assignments.

Orientation tuning width, SF, and TF characteristics

For each neuron located within PC ($n = 65$), DM ($n = 75$), or DP ($n = 48$), we carefully determined the location of the receptive field center and determined the optimal visual stimulus parameters for them. For each parameter measured below, there was considerable overlap, consistent with previous studies [e.g., Figure 2 in Koch's work (*13*)]. Despite this, we found significant differences in the population.

We fitted the CRF orientation tuning by a Gaussian function and calculated the width at half-height (WHH) of orientation tuning (Fig. 2A). As shown in Fig. 2D, there are highly significant differences in WHH between PC (mean ± SEM, 62° ± 3.1°) and DM (mean ± SEM, 48° ± 2.8°) neurons ($P < 0.01$, U test) and between PC and DP (mean ± SEM, 46° ± 3.4°) neurons ($P < 0.01$, U test). There was little difference in WHH between DM and DP neurons.

Using sinusoidal grating stimuli of different spatial frequencies drifted over the receptive field in the preferred orientation and direction, we determined the optimal SF of neurons in PC, DM, and DP locations (Fig. 2B). Figure 2E illustrates the optimal SF values of the neurons in PC (blue, $n = 53$), DM (green, $n = 63$), and DP (red, $n = 41$). The mean optimal SF of DP neurons (mean ± SEM, 0.45 ± 0.24 cycle/degree) was significantly lower than that of DM (mean ± SEM, 0.57 ± 0.28 cycle/degree; $P < 0.05$, U test) and PC neurons (mean ± SEM, 0.59 ± 0.29 cycle/degree; $P < 0.05$, U test); there is no significant difference between PC and DM neurons.

A previous study (*14*) reported the presence of PCs with low SF (0.2 cycle/degree) and those with high SF (0.6 cycle/degree). Our data also showed that the SF of PCs ranges from low to high (Fig. 2E). When we examined PCs in which more than one neuron was recorded ($n = 15$), we found, consistent with (*14*), that some PCs are of low SF (<0.4 cycle/degree; mean ± SD, 0.28 ± 0.09 cycle/degree; $n = 6$), while others are of high SF (>0.4 cycle/degree; mean ± SD, 0.75 ± 0.14 cycle/degree; $n = 9$) preference.
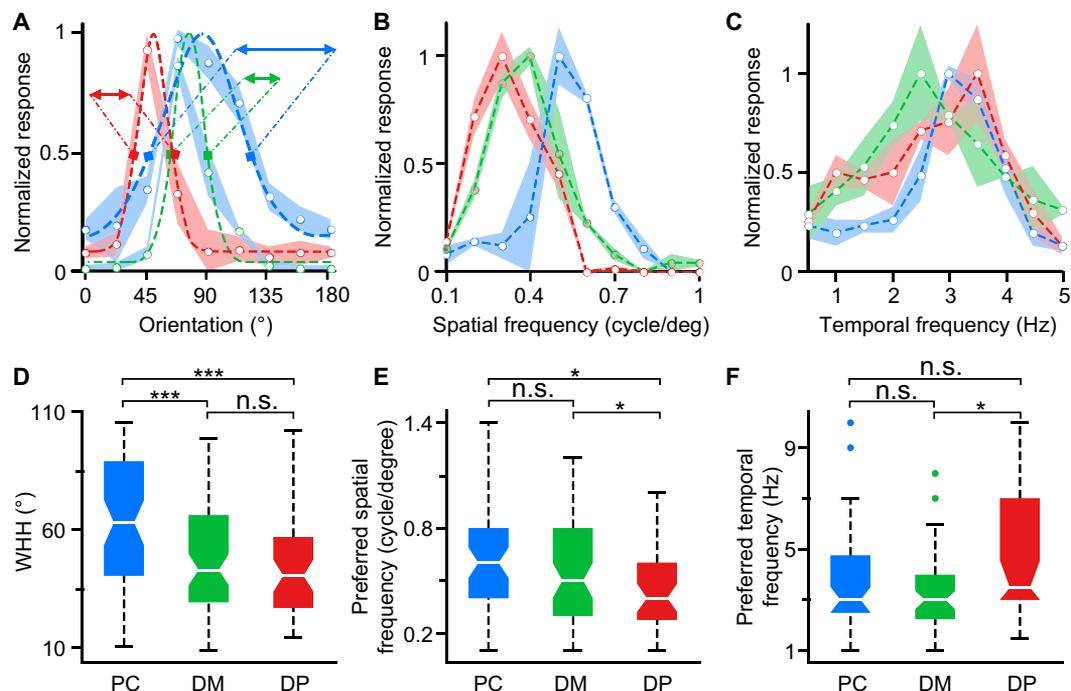
Fig. 2. Orientation tuning width, SF, and TF characteristics. (**A**) Orientation tuning curves of three cells located at PC (blue), DM (green), and DP (red) (color-coding same for all graphs). The tuning curves are fit with a Gaussian function (dashed lines). Horizontal arrows show WHH. (**B**) SF curves of three cells. The peak values show the optimal SF. (**C**) TF curves of three cells. The peak values show the optimal TF. Shadings in (A) to (C) represent the SDs. (**D** to **F**) Boxplots of WHH values and preferred SF and TF for PC, DM, and DP neurons. *, **, and *** represent the *P* values in individual comparison and are smaller than 0.05, 0.01, and 0.001 respectively. n.s., not significant.

Then, we compared the optimal TF preferences of DP, DM, and PC neurons using sine wave gratings drifted at optimal SF and different TFs (Fig. 2C). Contrary to the SF properties observed above, the data (Fig. 2F) revealed that the mean optimal TF of DP neurons (mean ± SEM, 4.66 ± 2.32 Hz; *n* = 35) was significantly higher than that of DM (mean ± SEM, 3.39 ± 1.65 Hz; *n* = 56; *P* < 0.05, *U* test). There is no significant difference between PC with DM and DP neurons.

Receptive field size and surround suppression strength
The spatial extent of the CRF and the strength of surround suppression were determined using size-tuning tests. Two types of responses were observed based on the absence or presence of surround suppression, i.e., surround nonsuppressive (SN; Fig. 3A) and surround suppressive (SS; Fig. 3B) patterns.

We examined the CRF size and surround suppression strength of cells of PC, DM, and DP locations. The CRF size is defined as the diameter of the saturation point (95% of the peak value, as in Fig. 3A) or as the peak response diameter (as in Fig. 3B). The degree of surround suppression was quantified by the surround suppression index (SI). This value is 0 for cells with no surround suppression and 1 for cells with 100% suppression.

CRF size
Figure 3D shows that, although many receptive fields fall within the 2° to 5° size range, the largest CRF sizes are present in regions away from PC, and the smallest CRF sizes are seen in PC locations. The CRF sizes in PC (mean ± SEM, 2.7° ± 0.2°; *n* = 58) is significantly different from DM (mean ± SEM, 3.4° ± 0.2°; *n* = 68; *P* < 0.05, *U* test) and DP (mean ± SEM, 4.4° ± 0.4°; *n* = 45; *P* < 0.01, *U* test) locations. There is no significant difference between DM and DP neurons. Thus, there appears to be a tendency for the largest receptive fields to be

located away from PCs and the smallest receptive fields (0° to 1°) to be located in PCs.

Surround suppression
Figure 3E shows that there was a tendency for neurons with stronger surround suppression to be located in PCs, and for cells with weakest surround suppression to be located away from PCs. Almost all (16 of 18) of the SN neurons (0 ≤ SI ≤ 0.1) were located in DP regions (only two SN neurons were located in DM regions). Comparison of the SI values of PC, DM, and DP neurons reveals that SI is highest in PC neurons (mean ± SEM, 0.55 ± 0.03; *n* = 58), although not significantly different from DM neurons (mean ± SEM, 0.52 ± 0.03; *n* = 68; *P* = 0.61, *U* test); however, SI was lowest in DP neurons (mean ± SEM, 0.30 ± 0.04; *n* = 45; PC versus DP, *P* < 0.001, *U* test; DM versus DP, *P* < 0.01, *U* test). We note that the total percentage of neurons with no surround suppression comprised roughly 10.5% (18 of 171), consistent with a previous study by Hashemi-Nezhad and Lyon (*15*) (11 of 117, 9.4%).

In summary, our data suggest that DM and DP neurons were differentiated with respect to strength of surround suppression, although they did not differ with respect to orientation tuning width. This indicated the importance of examining multiple functional properties for subdomain characterization.

Orientation tuning of the surround suppression
Having established that the strength of surround suppression (determined by the size-tuning tests) differs among neurons located in DP versus PC and DM regions, we next asked whether there is any relationship between the orientation selectivity of the center and the surround.

Surround suppressive properties were investigated on 146 neurons located at PC (*n* = 46), DM (*n* = 59), and DP (*n* = 41) positions;
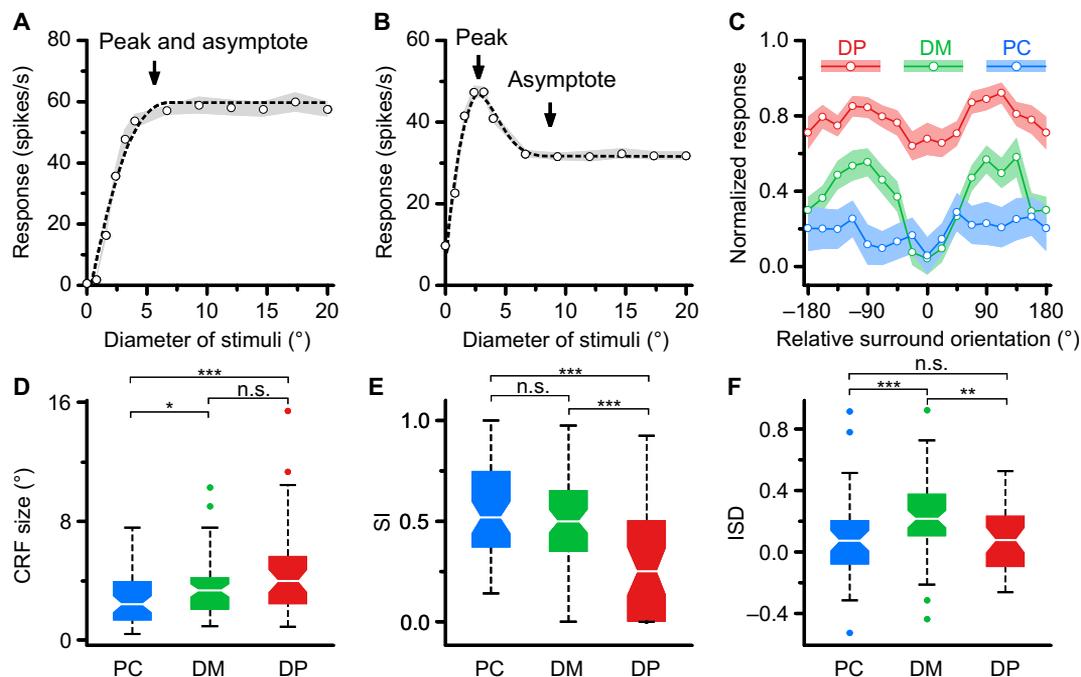
Fig. 3. CRF size, surround suppression strength, and surround orientation tuning. (**A** and **B**) The response in spikes per second (y axis) is plotted against the diameter of the circular grating patch (x axis). Dashed lines indicate the best-fitting Gaussian function integrals. Shadings represent the SDs. Arrows indicate stimulus diameter at which responses were maximal and asymptotic. (A) A cell (at location "3" in Fig. 1C) exhibiting no suppressive surround (SI = 0). (B) A cell (at location "1" in Fig. 1C) showing suppressive surround (SI = 0.38). (**C**) The average normalized tuning curves of surround for PC, DM, and DP neurons. The shadings represent ±SEM. (**D**) Boxplot of CRF size for PC, DM, and DP neurons. (**E**) Boxplot of SI for PC, DM, and DP neurons. (**F**) Boxplot of ISD for PC, DM, and DP neurons. *, **, and *** represent the P values in individual comparison are smaller than 0.05, 0.01, and 0.001 respectively. n.s., not significant.

the center stimulus was kept at the preferred orientation, while the surround orientation varied. As shown by the average normalized curves in Fig. 3C, the surround suppression profile differed between PC (blue curve), DM (green curve), and DP (red curve) neurons. The surround suppression at iso-orientation was similar for PC and DM cells, but for PC cells, the suppression at ortho-orientation was significantly stronger than that for DM neurons.

We consistently observed that the strength of iso-orientation relative to ortho-orientation surround suppression was stronger in DM compared to PC and DP neurons (see Fig. 3C). To quantify this observation, we used the index for iso-orientation suppression depth [ISD; (15)]. The boxplots of the ISD at PC (blue), DM (green), and DP (red) neurons are shown in Fig. 3F. Overall, the ISD values for DM neurons (mean ± SEM, 0.23 ± 0.03; n = 59) were significantly higher than those for PC (mean ± SEM, 0.08 ± 0.04; n = 46; P < 0.01, U test) and DP neurons (mean ± SEM, 0.09 ± 0.03; n = 41; P < 0.05, U test). Figure 3F shows that the surround orientation tuning in DM cells had higher selectivity, while the surround orientation selectivity was lower in PC and DP neurons.

With the method of two-photon calcium imaging in cat primary visual cortex, Ohki et al. (16) found the orientation map is highly ordered, even at the finest scale. They also found calcium dye response amplitudes in PCs were smaller (17 to 41%) than in the periphery and inferred that perhaps more complex stimuli, such as corners or other contextual stimuli, might be more effective (8). In our data, we found no difference between the average response rate of cells in PCs (30 ± 3.68 spikes/s, ±SD; n = 58) and iso-orientation domains (28 ± 3.5 spikes/s, ±SD; n = 113) for stimuli covering only the CRF; in contrast, the response rates to full-screen

stimuli (20°) were approximately 30% less in PCs (12 ± 2.15 spikes/s, ±SD; n = 58) than in orientation domain (DM and DP) cells (17 ± 2.1 spikes/s, ±SD; n = 113). Thus, these findings support the view that PC neurons have smaller receptive fields (Fig. 3D) and stronger surround suppression.

Response latency of neurons with surround suppression
Previous studies have reported that orientation-independent surround suppressed neurons had a shorter latency than did orientation-dependent surround suppressed neurons with single-unit recordings (17). As shown in Fig. 4, we examined the response latency of LFPs at DM (solid curve) and PC (dashed curves). Figure 4A shows the mean LFPs, and Fig. 4B shows the histogram distribution of response latency [time to peak; (11)]. Contrary to our expectation, the LFP response latency was significantly longer for PC sites (mean ± SEM, 88.23 ± 3.03 ms; n = 26) than DM sites (mean ± SEM, 74.5 ± 1.48 ms; n = 35; P < 0.01, U test), as reflected by both mean latency (Fig. 4A) and latency distribution (Fig. 4B).

We further compared the response latency of single neurons in PC and DM. We computed the mean peristimulus time histograms (PSTHs) of the neurons using single-cell recordings with surround suppression [similar to the analysis in (17)]. Figure 4C shows the mean normalized PSTH response curves, and Fig. 4D illustrates the histogram of latency (time from stimuli onset to 15% of the response peak). We again observed a longer mean latency to response for PC than for DM sites (Fig. 4C). As can be seen from Fig. 4D, the surround suppression latency of PC cells (mean ± SEM, 56.0 ± 4.56 ms; n = 29) was also significantly longer than that of DM cells (mean ± SEM, 39.8 ± 2.39 ms; n = 38; P < 0.01, U test).
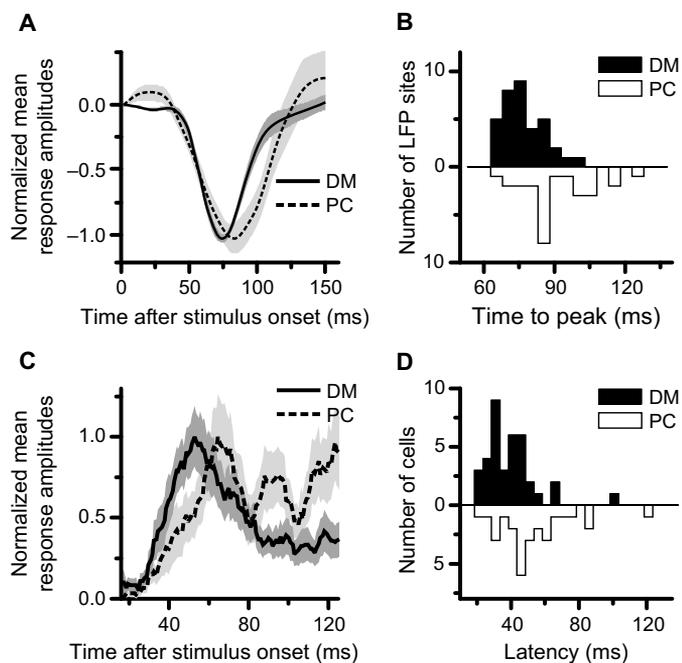
Fig. 4. Response latencies of DM and PC neurons. (**A**) The mean normalized LFP response curves of DM (solid lines) and PC (dashed lines) sites. Shadings represent the SEs. (**B**) Histogram distribution of response latencies (time to peak) at DM and PC. The time to peak of LFP at DM sites (mean ± SEM, 74.5 ± 1.48 ms; $n = 35$) is significantly shorter than that at PC sites (mean ± SEM, 88.2 ± 3.03 ms; $n = 26$; $P < 0.01$, U test). (**C**) The mean normalized single-unit PSTHs of DM (solid lines) and PC (dashed lines) neurons. Shadings represent the SEs. (**D**) The distribution of response latencies (time to 15% of the response peak) of complex neurons at DM and PC. The mean latency of DM neurons (mean ± SEM, 39.8 ± 2.39 ms; $n = 38$) is significantly shorter than that of PC neurons (mean ± SEM, 56.0 ± 4.56 ms; $n = 29$) ($P < 0.01$, U test).

DISCUSSION

Our systematic examination of neurons located within different parts of single orientation columns in cat V1 has revealed that orientation architectures are not uniform structures but can be divided into three functionally distinct subdomains: PC, DM, and DP. This determination is based on multiple functional criteria. Unlike previous studies (8–11, 15, 16, 18), which relied on a small number of functional parameters, we used a large battery of tests (receptive field size, orientation tuning width, SF, TF, surround suppression characteristics, and response latency) to classify and distinguish neuronal response within the orientation domain. These multiple criteria led us to identify a third subregion (DP) within orientation maps, located halfway between adjacent pinwheels. It is noteworthy that although there are significant differences between many (but not all) comparisons between these three zones for a single criterion, there remains much overlap, suggesting that, similar to orientation domains in V1, there is a gradation of selectivity between the three zones. Only when multiple criteria are considered together, these zones do appear to be differentiable.

In Fig. 5, we summarize our findings. The population of 171 neurons (58 in PC, 68 in DM, and 45 in DP) is displayed on a schematic divided into three concentric zones (PC, DM, and DP), with PC at the center. Each dot represents one neuron, with receptive field size represented by the size of the dot, the orientation preference by the angular position, the orientation homogeneity index [HI; a value of 1 indicates that the local pool of neurons is completely homogenous in their ori-

entation preferences, while a value of 0 indicates complete orientation heterogeneity (9)] by the radial position (white arrows: ranging from 0 to 1 within each of the three zones), and the SI by the color [color bar below: 0, no surround suppression (red); 1, strong surround suppression (blue)]. This representation illustrates the tendency for (i) the largest receptive fields to fall in the DP zone (large dots in Fig. 5) and the smallest receptive fields to fall in the PC zone (small dots in Fig. 5) (the receptive field size of the three types of neurons are compared in Fig. 3D), and (ii) the strongest surround suppression (blues) falling in the PC zones and the weakest in the DP zones (reds) (Fig. 3E). Although not included in this summary figure, we have also shown that (iii) PC zones have longer latency to response compared with DM zones (Fig. 4). Thus, PC, DM, and DP zones can be distinguished by multiple functional characteristics.

Despite this differentiation between subdomains, there is an overlap between PC, DM, and DP parameter distributions. This suggests that, similar to continuous shifting of orientation selectivity across orientation domains in V1, there is a gradation of selectivity across the three zones. It is noteworthy that since these three zones were identified on the basis of the selection of PC, DM, and DP points for data collection, they likely represent point within a continuum of change within the orientation domain. Challenging recording experiments with electrodes inserted horizontally across a single orientation domain (19) or finely spaced multielectrode arrays (13) would be needed to further examine this hypothesis.

Precise localization of PC, DM, and DP

While single-unit recording is the common method for studying columnar organization (2), it is quite challenging to show that the detailed characteristics differ systematically within different subdomains of a single column. This is due primarily to the poor localization accuracy of the extracellular recording method (20). Localization methods that rely on multielectrode (Utah) arrays, with 400-μm electrode spacing, have been used to infer pinwheel locations with accuracy (21) but have not resolved three-graded specializations of orientation domains. In this study, we applied many steps to assure the localization accuracy of electrodes (see Materials and Methods).

The weakness of targeting pinwheels based on vasculature is well recognized (10, 15, 16, 21). We overcame this issue by first assuring perpendicular penetrations (fig. S1) and then carefully targeting electrodes to PCs based on blood vessel guidance. This revealed two groups of penetrations: those with non–sine-like response and large scatter (>60°; (12)) in orientation preference (true PC locations) and those with sine-like LFP response and small scatter in orientation preference (not true PC locations); of 26 such penetrations, only 10 (38%) were truly in PC locations (Fig. 1F). This procedure revealed that PC penetrations with non–sine-like LFPs (NSI > 0.1; Fig. 1F) were locations of true PC locations. We subsequently used the non–sine-like criterion to determine PC locations (Fig. 1G).

Other methods have also been used to identify PC versus orientation domain locations. Hashemi-Nezhad and Lyon (15) used electrodes coated with DiI to demonstrate that electrodes were truly perpendicular; however, the vasculature-based method still contained localization error. Nauhaus and Ringach (21) carefully matched the electrode locations in a Utah array with locations in an optical imaged orientation map and achieved accurate PC localization; however, electrode spacings were 400 μm, insufficient for subdomain localization. An impressive two-photon study reported that the true PC is only 130 μm in diameter (16), underscoring the need for highly accurate electrode targeting
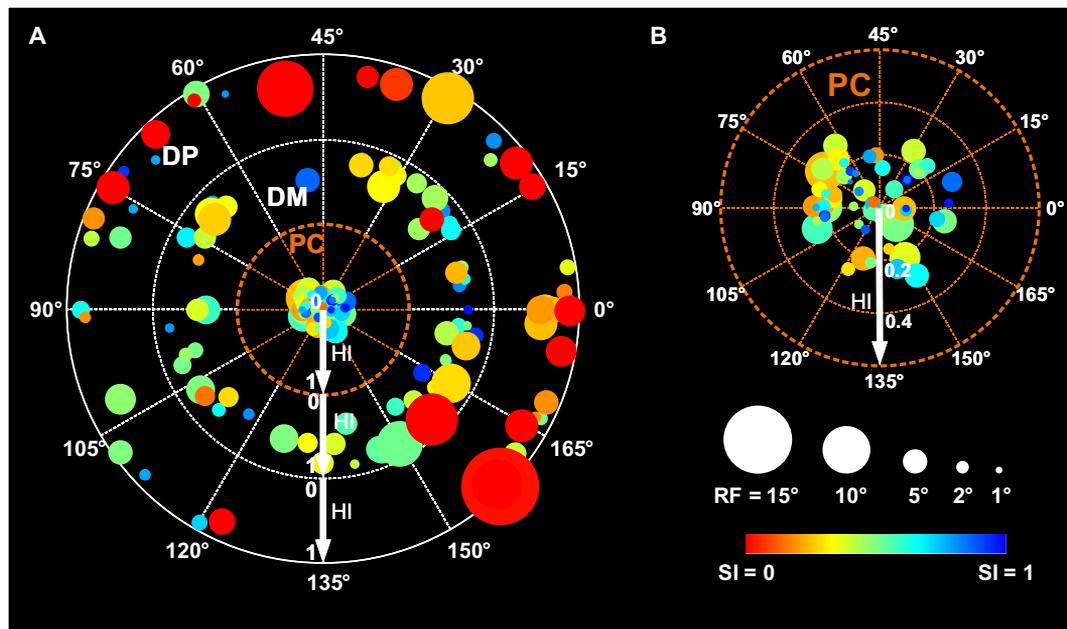
Fig. 5. Orientation column summary template of PC, DM, and DP neuron properties. (**A**) Orientation column template: The three concentric rings represent the subdomains of a pinwheel-like architecture centered on PC. Inner circle, PC; intermediate circle, DM; and outer circle, DP. Each dot represents one neuron. The circular position of each dot represents its orientation preference (angular coordinate). Radial position represents HI value (white arrows: 0 to 1 HI index for each zone). Dot size represents CRF size. Dot color represents value of SI (0 = no surround suppression, 1 = maximal surround suppression; color scale bar below). (**B**) Enlarged column template of the PC subdomain in (A). The size and color scale of the dots are identical to those in (A).

[see also (*10*)]. Perhaps two-photon imaging coupled with a large number of stimuli (*7*) could provide an optimal high-density map of orientation domain substructure.

Comparison with previous studies

Our results are largely consistent with previous studies but extend previous findings and suggest the presence of finer functional differentiation within single orientation domains than previously recognized. Similar to previous studies, we find (i) broader orientation tuning in PCs than in the periphery [Fig. 2D; cf. (*10*, *13*, *15*, *16*)], (ii) smaller receptive fields in PCs (Fig. 3D), and (iii) the presence of high SF and low SF preference PCs (*14*, *22*).

A new subdomain: DP

We have identified a new subdomain, DP, which is distinct from DM. This calls for a reevaluation of previous studies, two of which we highlight here. (i) Using the method of intrinsic signal optical imaging and single-unit recording in cat V1, Hashemi-Nezhad and Lyon (*15*) examined the surround suppression tuning in the traditional two areas (PC and iso-orientation domain) and found that the iso-orientation domain exhibits stronger orientation-selective surround suppression than PC. Our data suggest a new interpretation. Because we examined the suppression tuning in three areas (PC, DM, and DP), we found that, contrary to their study, there is no significant difference in ISD between DP and PC (Fig. 3F). (ii) Moreover, we find that DP shows much weaker orientation-selective surround suppression compared with DM (Fig. 3, C and F) and that DP contains almost all of the no surround suppression neurons (16 of 18). Thus, the distinguishing features of DP support the presence of distinct zones within orientation domains. DP's surround suppression properties are also suggestive of a key role in processing the linear aspects (as opposed to curves or corners) of contours. The implications are discussed below.

We believe our study provides insight into another previous study. Das and Gilbert (*8*) recorded cell pairs from within single orientation domains and reported that near iso-oriented cells have stronger suppression than far cells (29 of 31 cell pairs sampled), while a small number (2 of 31 cell pairs) had little effect. This resulted in the impression that very few cells have weak iso-oriented suppression. We suggest that their recordings, which were not systematically sampled, were biased toward PC and DM locations, thereby resulting in a bias toward neurons, which exhibit strong iso-orientation surround suppression (*n* = 29) and an undersampling of those in DP zones (*n* = 2). In our study (*n* = 171 neurons), we systematically recorded from three locations within the orientation domain producing comparable sampling (58 in PC, 68 in DM, and 45 in DP) and were therefore able to observe the predominance of weak surround suppression in the DP population (16 of 18 with no surround suppression). However, further study is needed to examine this suggestion.

Three subdomain architectures determined by multiple functional criteria

Previous studies have revealed that orientation domains and pinwheel regions are distinct regions of orientation representation. Orientation domains exhibit neurons with similar orientation preference (*1*, *16*), while pinwheels are locations of neurons with diverse tuning preference and greater plasticity (*8*, *13*, *18*). Using a large array of functional criteria, coupled with a novel method of subdomain localization, we find evidence for differentiation within the orientation domain.

On the basis of these findings, we propose a triple concentric model in which the pinwheel is at the center of three concentric regions containing neurons with different overall functional preferences. Note that this tripartite view is based on our sampling strategy and may reflect a continuum of change from PC to orientation domain center

(DP). We propose the pinwheel-based unit contains all the machinery for representing all orientations and elemental orientation integrations (from linear to curved to complex; see below). In this sense, we propose that the pinwheel-centered unit embodies the concept of an "orientation hypercolumn."

Proposed roles of DP, DM, and PC in detecting elemental visual features

As shown by this and other studies, neurons in DP locations are sharply tuned for orientation and are zones of homogeneous orientation (Fig. 6A). As these locations are linked to other orientation domains of similar orientation selectivity, they may represent iso-orientation networks that process linear oriented aspects of shape contours [morphology (23, 24–27) and function (28, 29)]. Consistent with this role of encoding the orientation of a linear contour segment, DP neurons exhibit large receptive fields that lack strong surround suppression and relatively lower SF preference (30).

Neurons in DM locations (Fig. 6B) are reminiscent of previously described end-stopped neurons, which were proposed to contribute to encoding of curvature. Some studies support the idea that V1 neurons with strong iso-orientation surround suppression (equivalent to our DM neurons) may contribute to detection of local discontinuities, including discontinuity in orientation (31–33), perceptual "pop-out," and illusory contours (6, 17, 34, 35).

Neurons in PC locations are quite distinct. They have the smallest receptive field sizes, the broadest orientation tuning curves, and are in locations where diverse orientation preferences converge (Fig. 6C). This diversity has led to proposals that PCs are locations of complex integration and synaptic plasticity [e.g., (13, 18)]. The longer latency to response at PCs is consistent with a higher-order stage of processing, which may contribute to encoding of more complex contour features. However, we note that some studies, using different stimuli for evaluating surround suppression, find shorter latency to response of orientation-independent surround suppression neurons (equivalent to PC locations

in this study) (17) relative to orientation-dependent surround suppression neurons. Thus, it is possible that PC neurons are dynamic and stimulus dependent, consistent with previous reports emphasizing synaptic plasticity at PC locations (18).

We summarize a model of the orientation domain circuit as it relates to these contour processing functions (Fig. 6D). DP, DM, and PC locations receive inputs (red arrows). In DP, contour orientation response is generated, resulting in loci of linear contour segment representation. This iso-oriented surround suppression (similar to end-stopping) may then confer curvature response to DM neurons. DMs of multiple orientation preference (green lines) then project to PC locations where more complex integrations occur.

MATERIALS AND METHODS
Animal preparation
This study was performed in strict accordance with the recommendations contained in the *Guide for the Care and Use of Laboratory Animals* of the National Institutes of Health and approved by the Committee on the Ethics of Animal Experiments of the Shanghai Institute for Biological Sciences, Chinese Academy of Sciences (permit no. ER-SIBS-621001C).

Acute experiments were performed on 16 cats of both sexes, 5 cats for verifying the validity of the confidence level setting (Fig. 1) and 11 cats for comparing the functional characteristics of neurons in PC, DM, and DP regions (Figs. 1 to 5). Detailed descriptions of procedures for animal surgery, anesthesia, and recording techniques can be found in previous studies (36). Briefly, cats were anesthetized before surgery with ketamine hydrochloride (30 mg/kg), and then tracheal and venous cannulations were performed. After surgery, the animal was placed in a stereotaxic frame for performing a craniotomy and conducting neurophysiological procedures. During recording, anesthesia and paralysis were maintained with urethane (20 mg/kg per hour) and gallamine triethiodide (10 mg/kg per hour), and glucose (200 mg/kg
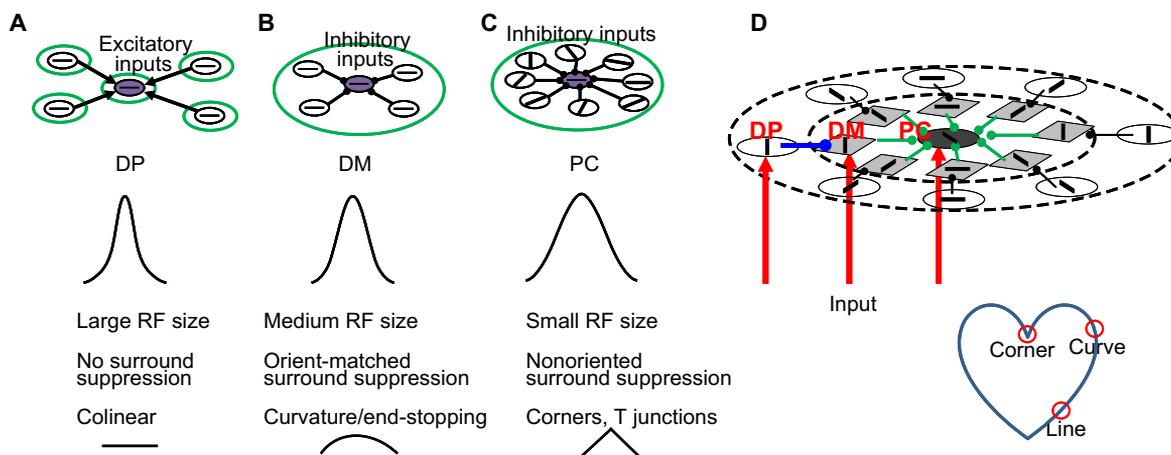

Fig. 6. Model depicting proposed three components of contour processing. (**A** to **C**) Top row: Oriented neurons (black ovals with oriented line segments) within orientation subdomains [green ovals: (A) DP subdomain, (B) DM subdomain, and (C) PC subdomain]. Middle row: Schematic orientation tuning curves for DP, DM, and PC neurons. Bottom row: Functional characteristics of DP, DM, and PC neurons and their proposed roles in contour processing (straight, curved, and corner symbols at the bottom). (A) DP subdomains are linked to other DP subdomains of similar orientation selectivity. This represents an iso-orientation network. (B) DM subdomains receive inhibitory input from similarly oriented neurons in the same orientation column. (C) PC subdomains receive inhibitory input from differently oriented columns. (**D**) Model of the orientation organization circuit as it relates to contour processing. DP, DM, and PC locations receive inputs (red arrows). DP, locus of linear contour segment representation; DM, orientation-dependent suppression from DP inputs (blue); PC, orientation-independent suppression from DM inputs (green). Bottom: Red circles indicate different parts of a heart shape image that would be processed by DP (line), DM (curve), and PC (corner). Arrows, excitatory inputs; line with dot, inhibitory input.

per hour) in Ringer's solution (3 ml/kg per hour) was infused. Heart rate, electrocardiography, electroencephalography (EEG), end-expiratory CO2, and rectal temperature were monitored continuously. Anesthesia was considered to be sufficient when the EEG indicated a stable sleep-like state marked by sleep spindles. Reflexes, including cornea and eyelid, and withdrawal reflexes were tested at appropriate intervals. The nictitating membranes were retracted, and the pupils were dilated. Contact lenses and additional corrective lenses were applied to focus the retina on a screen during stimulus presentation. A craniotomy was made above area 17 (V1), and a stainless steel chamber was cemented.

Following durotomy, the chamber was sealed with a coverglass and filled with silicone oil. In some experiments, no chamber was used, and the cortex was covered with agar and a coverglass. At the end of the experiment, the animal was euthanized by an overdose of barbiturate administered intravenously (dosage, 5 ml; 6% barbiturate).

Optical imaging

Optical images were captured with a 14-bit video camera (iXon DU-897, Andor Technology, Northern Ireland) consisting of a 512×512 pixel array of and equipped with two front-to-front connected 50-mm Nikon lenses, positioned over the exposed cortex. A reference map of the blood vessel pattern (see Fig. 1A) was obtained using green light (546 nm). The camera was then focused ~400 μm below the surface of the cortex, and data were collected using red light at 605 nm. To obtain orientation preference maps, the intrinsic signals were recorded in response to binocularly viewed full-screen, high-contrast (100%) sine wave gratings (0.5 cycles/degree) drifting at a TF of 2 Hz. The main set of stimuli included drifting gratings, presented at eight equally spaced orientations, in both directions (16 conditions). Each stimulus was presented 20 times for 9 s, followed by an interstimulus interval of 16 s. The visual stimuli were generated by a Cambridge Systems VSG graphics board and presented on a high-resolution monitor screen (40 cm by 30 cm) at a 100-Hz vertical refresh rate. The screen background was maintained at the identical mean luminance as the stimulus patches (10 cd/m^2). The monitor was placed 57 cm from the cat's eyes. Color-coded orientation preference maps (Fig. 1B) were generated by pixel-by-pixel vector summation of the eight orientations (1). In some experiments, drifting gratings were presented at 16 equally spaced orientations (at 11.25° intervals). We were very careful to choose only highly accurate and reproducible maps. We used map locations in which there was no displacement of PCs between maps generated from different subsets of trials (9). We used orientation map regions where orientation domains and pinwheels were congruent between these maps.

Determining the PCs

PCs were preliminarily targeted on the basis of surface blood vessel pattern aligned to the orientation map (see Fig. 1, A and B). The electrode penetrations were made perpendicular to the cortical surface, recording the LFP orientation tunings and calculating the NSI. Within the very local region around the preliminary PC, we made multiple penetrations until a non–sine-like LFP curve was obtained (NSI > 0.10), and then the electrodes could precisely locate the immediate vicinity of the PCs.

Locating the positions of electrodes

After determining the electrode positions of the PCs (points 1 and 2), recorded stereotaxically (Narishige, Japan), the midpoint between the

two adjacent PCs (DP, point 3) was determined by calculating the geometric midpoint of these stereotaxic coordinates. The midpoints between the PC and DP (DM, points 4 and 5) were similarly determined (see Fig. 1C).

Electrophysiology

Cells were recorded in the superficial cortex (within the first 600 μm). Single-cell recordings were made with tungsten-in-glass microelectrodes (37), and the impedance of the electrodes was about 5 megohms (tip diameter about 1 μm). We took extra efforts to ensure that the electrode penetration was perpendicular to the cortical surface. First, to ensure the camera's angle was exactly perpendicular to the plane of the cortex, we imaged a large field of view with a narrow depth of field [~50 μm, back-to-back lens with f1.2 (38)]. We then ensured the electrode paralleled the axis of the optical imaging. Using this procedure, we have estimated that the deviation of electrodes from perpendicular is less than 2° (see fig. S1). Once the electrode was inserted, the chamber surrounding the craniotomy was filled with 2% agar solution in saline. Electrodes were advanced through the cortex by a hydraulic Microdrive (Narishige, Japan). The signals were recorded using the Cerebus System. Spike signals were band-pass filtered at 250 to 7500 Hz and sampled at 30 kHz. Only well-isolated cells satisfying the strict criteria for single-unit recordings (fixed shape of the action potential and the absence of spikes during the absolute refractory period) were recorded for further analyses.

All cells recorded were located in the area of the cortex representing the central 10° of the visual field. When the single-cell action potentials were isolated, the preferred orientation, SF, and TF of each cell were determined. Each cell was stimulated monocularly through the dominant eye, with the nondominant eye occluded.

To locate the center of the CRF, a narrow rectangular sine wave grating patch (0.5° to 1.0° wide, 3.0° to 5.0° long, 100% contrast) was moved at successive positions along axes perpendicular or parallel to the optimal orientation of the cell, and the response to its drift was measured. The grating was set at the optimal orientation and SF and drifted in the preferred direction at the optimal speed for the recorded cells. The peak of the response profiles for both axes was defined as the center of the CRF. We determined the size of the CRF by performing an occlusion test, in which a mask consisting of a circular blank patch and concentric with the CRF was gradually increased in size on a background drifting grating (19, 36, 39, 40).

We tested the CRF orientation tuning. For each tuning curve, we fitted a Gaussian function and then determined the preferred orientation and the WHH (41). The visual stimuli of the LFP recording were 10° sine wave grating at 50% contrast, and the pseudorandom sequences of gratings of varying orientation and spatial phase, each for LFP, flashed for 32 ms (orientation noise stimulus). To analyze stimulus-evoked LFP responses, we filtered the recordings between 3 and 100 Hz and computed z scores by averaging responses across trials [for more details, see Figure 1 of (11)]. By testing LFP orientation tuning, we were able to derive the parameter of the NSI. In the size-tuning tests, the circular sinusoidal gratings (100% contrasts) were centered over the receptive field center and randomly presented with different diameters (from 0.1° to 20°). The optimized values for these parameters (orientation, SF, and TF) were used in these tests.

Each grating size was presented for 5 to 10 cycles of grating drift, and SEs were calculated for 3 to 10 repeats. We defined the CRF size as the aperture size of the peak response diameter (the stimulus diameter at which the response was maximal if the responses decreased at

larger stimulus diameters or reached 95% of the peak value if they did not). We quantified the degree of surround suppression for each cell using the SI (SI = 1 − asymptotic response/peak response). The cells were classified as "simple" if the first harmonic (F1) of their response to the sine wave gratings was greater than the mean firing rate (F0) of the response (F1/F0 ratio > 1), or "complex" if the F1/F0 ratio was <1 (42). The vast majority of our cells were complex.

To measure the orientation tuning of the cell's surround, the optimal orientation, aperture, and spatiotemporal frequencies for the center stimulus remained constant. Directly abutting the outer circumference of the center stimulus was a surround grating (with an outer diameter of 20°) of the identical phase, SF, and TF. Whereas the center stimulus was maintained at the preferred orientation/direction throughout the experiment, the surround stimulus was presented with variable orientations (in 22.5° increments). Both the center and surround stimuli were shown at a high contrast (100%). The responses to each patch were recorded for 5 to 10 cycles of the grating drift, and SEs were calculated for 3 to 10 repeats.

Data analysis
Classic receptive field size and SI
For determining the receptive field size and SI, we used the so-called difference of Gausians (DOG) model to fit the size-tuning curves (40). In this model, two Gaussians curves were concentrically overlapping, and the summation profile could be represented as the difference of the two Gaussian integrals. The model is defined by the following function

$$R(x) = R_0 + K_e \int e^{-(2x/a)^2} dx - K_e \int e^{-(2x/b)^2} dx$$

where x is the diameter of the stimulus and $R(x)$ is the response magnitude of the cell at the stimulation size of x. From this function, two parameters could be extracted: x_{peak} (stimulus diameter at which the response was maximal) and $x_{asymptotic}$ (stimulus diameter at which responses stabilized). The CRF and SI were defined by the following equations

$$\begin{cases} CRF = x_{peak} \\ SI = 1 - R(x_{asymtotic})/R(x_{peak}) \end{cases}$$

Homogeneity index
The homogeneity of orientation preference of the local environment for each recording site on the orientation map was quantified by the HI, as described in (10, 15). The HI for a cortical location x is defined as

$$HI(x) = \frac{1}{2\pi\delta^2} \left| \int \exp\left(\frac{-\|x - y\|^2}{2\delta^2}\right) \exp(2\theta_y i) dy \right|$$

where θ_y is the orientation preference at site y and δ determines the spread of the spatial scale. We used a value of $\delta = 180$ μm to match the spatial extent of the basal dendritic spread of V1 neurons. An index value of 1 indicates that the local pool of neurons is completely homogenous in their orientation preferences, while a value of 0 indicates complete orientation heterogeneity.

Iso-orientation suppression depth
ISD is a measure of the depth of center suppression by an iso-oriented surround, relative to the average depth of suppression from the two

orthogonal surrounds (15)

$$ISD = \frac{(R_{\theta-90} + R_{\theta+90} - 2R_{\theta0})}{2R_{ref}}$$

where $R_{\theta0}$ represents the response magnitude at iso-orientation, $R_{\theta-90}$ and $R_{\theta+90}$ represent the response magnitude for the two orthogonal orientations, and R_{ref} is the response to the center stimulus presented alone.

Non–sine-like index
To estimate the unlikeness of a curve to sine waves, we proposed NSI, which is defined as the P value in a surrogate data test. Considering an LFP orientation-tuning curve C_0, use q_0 to denote its fitting error to sine models. Make the null hypothesis (H_0) that C_0 is non–sine-like and use Γ to denote the statistical distribution of the fitting error under H_0. In other words, if H_0 holds, q_0 should be one of the samples of Γ, and if q_0 is significantly smaller than the samples of Γ, we would reject H_0 and conclude that C_0 is sine-like. Because it is hard to estimate the distribution Γ directly, here we use the surrogate data method (43, 44) to obtain a surrogate distribution (Γ') and then test whether q_0 is a sample from Γ' or not. To do this, we randomly shuffled the eight sample points (at eight orientations) of the curve (C_0) N times (44) and obtained N surrogate non–sine-like curves (denoted by C_i, $1 \leq i \leq N$, $N = 1000$), then fit each surrogate curve (C_i) to sine models and used q_i ($1 \leq i \leq N$) to denote the fitting error. Γ' is constructed by counting q_i, and the P value was calculated as the percentage of q_i, which is smaller than q_0. Then, NSI is defined as the P value. It ranged from 0 to 1, with 0 as highly sine-like and 1 as highly non–sine-like.

Multiple comparison
For the functional parameters of orientation tuning width, spatiotemporal frequency preference, receptive field size, surround SI, ISD, and latency to response, the differences between PC, DM, and PC were first examined by Mann-Whitney U test individually. Then, the P values were corrected by the Benjamini-Hochberg procedure to control for false discovery rate of multiple comparisons (45).

SUPPLEMENTARY MATERIALS
Supplementary material for this article is available at http://advances.sciencemag.org/cgi/content/full/5/6/eaaw0807/DC1
Fig. S1. Ensuring the electrode is perfectly perpendicular to cortical surface.

REFERENCES AND NOTES
1. T. Bonhoeffer, A. Grinvald, Iso-orientation domains in cat visual cortex are arranged in pinwheel-like patterns. *Nature* **353**, 429–431 (1991).
2. D. H. Hubel, T. N. Wiesel, Sequence regularity and geometry of orientation columns in the monkey striate cortex. *J. Comp. Neurol.* **158**, 267–293 (1974).
3. D. E. Wilson, D. E. Whitney, B. Scholl, D. Fitzpatrick, Orientation selectivity and the functional clustering of synaptic inputs in primary visual cortex. *Nat. Neurosci.* **19**, 1003–1009 (2016).
4. S. Grossberg, Cortical dynamics of figure-ground separation in response to 2D pictures and 3D scenes: How V2 combines border ownership, stereoscopic cues, and gestalt grouping rules. *Front. Psychol.* **6**, 2054 (2016).
5. D. H. Hubel, T. N. Wiesel, Receptive fields and functional architecture In two nonstriate visual areas (18 and 19) of the cat. *J. Neurophysiol.* **28**, 229–289 (1965).
6. J. J. Knierim, D. C. van Essen, Neuronal responses to static texture patterns in area V1 of the alert macaque monkey. *J. Neurophysiol.* **67**, 961–980 (1992).
7. S. Tang, T. S. Lee, M. Li, Y. Zhang, Y. Xu, F. Liu, B. Teo, H. Jiang, Complex pattern selectivity in macaque primary visual cortex revealed by large-scale two-photon imaging. *Curr. Biol.* **28**, 38–48.e3 (2017).

8. A. Das, C. D. Gilbert, Topography of contextual modulations mediated by short-range interactions in primary visual cortex. *Nature* **399**, 655–661 (1999).

9. J. Mariño, J. Schummers, D. C. Lyon, L. Schwabe, O. Beck, P. Wiesing, K. Obermayer, M. Sur, Invariant computations in local cortical networks with balanced excitation and inhibition. *Nat. Neurosci.* **8**, 194–201 (2005).

10. I. Nauhaus, A. Benucci, M. Carandini, D. L. Ringach, Neuronal selectivity and local map structure in visual cortex. *Neuron* **57**, 673–679 (2008).

11. S. Katzner, I. Nauhaus, A. Benucci, V. Bonin, D. L. Ringach, M. Carandini, Local origin of field potentials in visual cortex. *Neuron* **61**, 35–41 (2009).

12. P. E. Maldonado, I. Gödecke, C. M. Gray, T. Bonhoeffer, Orientation selectivity in pinwheel centers in cat striate cortex. *Science* **276**, 1551–1555 (1997).

13. E. Koch, J. Jin, J. M. Alonso, Q. Zaidi, Functional implications of orientation maps in primary visual cortex. *Nat. Commun.* **7**, 13529 (2016).

14. M. Hübener, D. Shoham, A. Grinvald, T. Bonhoeffer, Spatial relationships among three columnar systems in cat area 17. *J. Neurosci.* **17**, 9270–9284 (1997).

15. M. Hashemi-Nezhad, D. C. Lyon, Orientation tuning of the suppressive extraclassical surround depends on intrinsic organization of V1. *Cereb. Cortex* **22**, 308–326 (2012).

16. K. Ohki, S. Chung, P. Kara, M. Hübener, T. Bonhoeffer, R. C. Reid, Highly ordered arrangement of single neurons in orientation pinwheels. *Nature* **442**, 925–928 (2006).

17. H.-C. Nothdurft, J. L. Gallant, D. C. Van Essen, Response modulation by texture surround in primate area V1: Correlates of "popout" under anesthesia. *Vis. Neurosci.* **16**, 15–34 (1999).

18. V. Dragoi, C. Rivadulla, M. Sur, Foci of orientation plasticity in visual cortex. *Nature* **411**, 80–86 (2001).

19. H. S. Yao, C. Y. Li, Clustered organization of neurons with similar extra-receptive field properties in the primary visual cortex. *Neuron* **35**, 547–553 (2002).

20. J. C. Horton, D. L. Adams, The cortical column: A structure without a function. *Phil. Trans. R. Soc. Lond. B Biol. Sci.* **360**, 837–862 (2005).

21. I. Nauhaus, D. L. Ringach, Precise alignment of micromachined electrode arrays with V1 functional maps. *J. Neurophysiol.* **97**, 3781–3789 (2007).

22. D. Shoham, M. Hübener, S. Schulze, A. Grinvald, T. Bonhoeffer, Spatio-temporal frequency domains and their relation to cytochrome oxidase staining in cat visual cortex. *Nature* **385**, 529–533 (1997).

23. A. Angelucci, J. B. Levitt, E. J. S. Walton, J.-M. Hupé, J. Bullier, J. S. Lund, Circuits for local and global signal integration in primary visual cortex. *J. Neurosci.* **22**, 8633–8646 (2002).

24. Y. J. Liu, M. U. Ehrengruber, M. Negwer, H. J. Shao, A. H. Cetin, D. C. Lyon, Tracing inputs to inhibitory or excitatory neurons of mouse and cat visual cortex with a targeted rabies virus. *Curr. Biol.* **23**, 1746–1755 (2013).

25. R. Malach, Y. Amir, M. Harel, A. Grinvald, Relationship between intrinsic connections and functional architecture revealed by optical imaging and in vivo targeted biocytin injections in primate striate cortex. *Proc. Natl. Acad. Sci. U.S.A.* **90**, 10469–10473 (1993).

26. D. Y. Ts'o, C. D. Gilbert, T. N. Wiesel, Relationships between horizontal interactions and functional architecture in cat striate cortex as revealed by cross-correlation analysis. *J. Neurosci.* **6**, 1160–1170 (1986).

27. T. Yousef, E. Tóth, M. Rausch, U. T. Eysel, Z. F. Kisvárday, Topography of orientation centre connections in the primary visual cortex of the cat. *Neuroreport* **12**, 1693–1699 (2001).

28. V. Bringuier, F. Chavane, L. Glaeser, Y. Frégnac, Horizontal propagation of visual activity in the synaptic integration field of area 17 neurons. *Science* **283**, 695–699 (1999).

29. D. J. Field, A. Hayes, R. F. Hess, Contour integration by the human visual system: Evidence for a local "association field". *Vision Res.* **33**, 173–193 (1993).

30. T. Xu, H.-M. Yan, X. M. Song, M. Li, Y.-J. Li, Silent suppressive surrounds and optimal spatial frequencies of single neurons in cat V1. *Neurosci. Lett.* **597**, 104–110 (2015).

31. Z. M. Shen, W.-F. Xu, C.-Y. Li, Cue-invariant detection of centre-surround discontinuity by V1 neurons in awake macaque monkey. *J. Physiol.* **583**, 581–592 (2007).

32. A. M. Sillito, K. L. Grieve, H. E. Jones, J. Cudeiro, J. Davis, Visual cortical mechanisms detecting focal orientation discontinuities. *Nature* **378**, 492–496 (1995).

33. T. Xu, L. Wang, X.-M. Song, C.-Y. Li, The detection of orientation continuity and discontinuity by cat V1 neurons. *PLOS ONE* **8**, e79723 (2013).

34. V. A. Lamme, The neurophysiology of figure-ground segregation in primary visual cortex. *J. Neurosci.* **15**, 1605–1615 (1995).

35. R. von der Heydt, E. Peterhans, Mechanisms of contour perception in monkey visual cortex. I. Lines of pattern discontinuity. *J. Neurosci.* **9**, 1731–1748 (1989).

36. X.-M. Song, C.-Y. Li, Contrast-dependent and contrast-independent spatial summation of primary visual cortical neurons of the cat. *Cereb. Cortex* **18**, 331–336 (2008).

37. C.-Y. Li, X.-Z. Xu, D. Tigwell, A simple and comprehensive method for the construction, repair and recycling of single and double tungsten microelectrodes. *J. Neurosci. Methods* **57**, 217–220 (1995).

38. E. H. Ratzlaff, A. Grinvald, A tandem-lens epifluorescence macroscope: Hundred-fold brightness advantage for wide-field imaging. *J. Neurosci. Methods* **36**, 127–137 (1991).

39. C.-Y. Li, W. Li, Extensive integration field beyond the classical receptive field of cat's striate cortical neurons—Classification and tuning properties. *Vision Res.* **34**, 2337–2355 (1994).

40. J. B. Levitt, J. S. Lund, The spatial extent over which neurons in macaque striate cortex pool visual signals. *Vis. Neurosci.* **19**, 439–452 (2002).

41. N. V. Swindale, Orientation tuning curves: Empirical description and estimation of parameters. *Biol. Cybern.* **78**, 45–56 (1998).

42. B. C. Skottun, R. L. De Valois, D. H. Grosof, J. A. Movshon, D. G. Albrecht, A. B. Bonds, Classifying simple and complex cells on the basis of response modulation. *Vision Res.* **31**, 1079–1086 (1991).

43. J. Theiler, S. Eubank, A. Longtin, B. Galdrikian, J. D. Farmer, Testing for nonlinearity in time series: The method of surrogate data. *Physica D* **58**, 77–94 (1992).

44. J. A. Scheinkman, B. Lebaron, Nonlinear dynamics and stock returns. *J. Bus.* **62**, 311–337 (1989).

45. Y. Benjamini, Y. Hochberg, Controlling the false discovery rate: A practical and powerful approach to multiple testing. *J. R. Stat. Soc. Series B* **57**, 289–300 (1995).

Citation: M. Li, X. M. Song, T. Xu, D. Hu, A. W. Roe, C.-Y. Li, Subdomains within orientation columns of primary visual cortex. *Sci. Adv.* **5**, eaaw0807 (2019).

Science Advances

Subdomains within orientation columns of primary visual cortex

Ming Li, Xue Mei Song, Tao Xu, Dewen Hu, Anna Wang Roe and Chao-Yi Li

ARTICLE TOOLS	http://advances.sciencemag.org/content/5/6/eaaw0807
SUPPLEMENTARY MATERIALS	http://advances.sciencemag.org/content/suppl/2019/06/03/5.6.eaaw0807.DC1
REFERENCES	This article cites 45 articles, 8 of which you can access for free http://advances.sciencemag.org/content/5/6/eaaw0807#BIBL
PERMISSIONS	http://www.sciencemag.org/help/reprints-and-permissions

Use of this article is subject to the Terms of Service